SS-141
2660.0

A PROPOSAL TO BRING AN INTERIM BUBBLE CHAMBER TO NAL

N. Gelfand
University of Chicago

A. Pevsner
Johns Hopkins University

and

P. Slattery
University of Rochester

ABSTRACT

This report assumes that the 25-ft bubble chamber will ultimately be built for NAL but that it will not be available for a program of strong-interaction physics until a few years after experimental beams become operational. The possibility of making use of an existing chamber in the interim is discussed. The specific proposal is made to move the 80-in. BNL chamber to NAL and to increase its magnetic field to 30-35kG.

I. SELECTION OF AN INTERIM CHAMBER

The purpose of this report is to discuss the desirability of bringing to NAL during its initial period of operation a presently existing United States bubble chamber for the purpose of carrying out a limited program of strong-interaction physics at the higher energies made available for the 200-GeV accelerator. The motivation for this study is the possibility that the construction of the 25-ft bubble chamber may be delayed by fiscal and/or technical difficulties beyond the date when beams become available in the NAL experimental areas. An additional consideration is the possibility that conflicts could arise between the requirements of the neutrino and the hadron physics programs for the 25-ft chamber and that these conflicts could lead to a further postponment of the strong-interaction physics program for this chamber. For these reasons we have considered each of the bubble chambers now in operation in the United States with the goal of determining their utility in the 50 GeV/c region of projectile momenta.

This report should not be interpreted as proposing an alternative to the 25-ft bubble chamber for the purpose of analyzing strong interactions. Unless the

performance of the 25-ft bubble chamber is considerably below expectations, that chamber will possess a unique capability for strong-interaction physics which cannot be duplicated by any smaller device. Moreover, it appears clear that no new chamber could be designed, proposed, approved, and constructed in time to be available during the interim period being considered in this report.

We shall restrict our attention in this report to just the three chambers listed in Table 1. Should it become desirable, however, to consider moving to NAL some other existing chamber, then a similar analysis could also be used to evaluate the technical desirability of such a decision. It is envisioned that the ultimate choice of which chamber to move will be deferred to the latest time compatible with the chamber being operational when NAL experimental beams become available. In this way the final decision could be readily delayed to take into account additional data which should soon become available concerning the larger chambers, and which could have an important influence on some of the arguments presented in this report.

Table 1 was restricted to just three chambers for the following reasons. The SLAC 40-in. chamber is representative of the small chambers in current operation, and moreover a program of chamber improvement has already been proposed at SLAC for this chamber during which its magnetic field would be increased to 70 kG, and an effort would be made to decrease its setting error below 50μ. Consequently, in its modified form this chamber would appear to be nearly optimized for a device of its size.

For larger chambers in the two-meter range we could in principle have chosen from three candidates: the BNL 80-in. chamber, the SLAC 82-in. chamber, and the BNL 7-ft test chamber. Our reasons for choosing to discuss the BNL 80-in. chamber may be summarized as follows. In comparison with the SLAC 82-in. chamber, the BNL 80-in. chamber has more than three times as much volume due to its larger cross-sectional area. Furthermore, the 80-in. chamber would appear to be more easily spared by its parent laboratory since without the 82-in. chamber SLAC would be left with no large bubble chamber with which to carry out its very important current bubble-chamber physics program. In contrast, a successfully operating 7-ft chamber would provide BNL with two large chambers, one of which could presumably be spared if this were to be justified by its physics potential at NAL. The reasons for choosing the BNL 80-in. chamber rather than the 7-ft were first that the former chamber appears at this time to be the more accurate of the two chambers, and, second, BNL has proposed an expansion program for the 7-ft chamber which would improve its usefulness for neutrino physics at BNL, and, hence, from the point of view of maximizing the total national high-energy physics capability, make it less

transferable than the 80-in. These reasons notwithstanding, however, in the context of this report, the BNL 80-in. chamber may be regarded as representing all three two-meter chambers.

Finally, in the realm of larger chambers, only the ANL 12-ft and the BNL modified 7-ft chambers can be expected to be in operation when NAL starts up. We have chosen to discuss the ANL 12-ft chamber because it possibly might be more easily spared by its parent laboratory.

II. INTERACTIONS AND CONSTRAINTS

The first point which becomes apparent when considering the study of strong-interaction physics in an existing bubble chamber at NAL energies is that not all classes of reactions will be accessible. For example, events with missing neutrals are already difficult to analyze at presently achievable energies and will become increasingly more difficult as beam momenta are increased. In fact, it is far from certain that at NAL energies such physics will be fully analyzable in any bubble chamber unless γ's are converted and π^o momenta reconstructed directly.

A second point is that decays of fast secondaries are also going to be increasingly difficult to analyze: kink angles are going to become even more minute, and decay lengths will be getting increasingly longer. For example, a 40 GeV/c K_s will have a decay length of over 2 meters.

For these reasons we have chosen to restrict our attention in this report to single-vertex four-constraint interactions. This it not meant to imply that other interesting investigations cannot be carried out at NAL with the chambers being herein considered. For example, general survey experiments involving the analysis of unfitted charged secondary tracks will be of considerable interest in the high-energy region. Such studies can be most conveniently made in a bubble chamber and should be carried out during the initial period of NAL operation. It is, however, our conviction that much interesting physics will lie in the realm of four-constraint interactions and that a strong case can be made for bringing an interim chamber to NAL based upon a demonstration of its capability for analyzing just this restricted reaction class.

For example, one very interesting class of reactions which could be studied with a chamber chosen primarily for its ability to analyze one-vertex four-constraint interactions is diffraction dissociation, of which a typical example is:

$$\pi^{\pm} p \rightarrow A_1^{\pm} p$$
$$\hookrightarrow \pi^{\pm} \rho^o$$
$$\hookrightarrow \pi^+ \pi^- .$$

By studying the high-energy properties of such reactions as a function of beam momentum, one can reasonably hope to learn much more than one could discover from merely carrying out higher-statistics experiments at presently accessible energies. Since the 200-GeV accelerator will for the first time make accessible to U. S. physicists p-p collisions above ~ 30 GeV/c, π-p collisions above ~ 25 GeV/c, and $\bar{p}$-p and K-p collisions above ~20 GeV/c (the present limit for K-p collisions is only 13 GeV/c), there are many other examples of equally analyzable four-constraint reactions whose high-energy behavior should prove sufficiently interesting to justify the relatively moderate expense of providing an interim bubble chamber for NAL.

Before it is possible to carry out a quantitative analysis of the ability of existing bubble chambers to analyze one-vertex four-constraint events in the range of beam momenta below 50 GeV/c, it is necessary to assume a model for such reactions. In this report we shall make the following assumptions:

1. The distribution of transverse momenta for secondary particles produced in high-energy collisions is described by an approximately beam-momentum independent function:

$$\overline{\Pi}(p_T) = \frac{p_T e^{-p_T/0.16}}{\int_0^{p_T^{max}} p_T e^{-p_T/0.16}\, dp_T}, \qquad (1)$$

where $\overline{\Pi}(p_T)$ is the probability that a given secondary particle has transverse momentum p_T,

p_T is measured in GeV/c,

p_T^{max} is the maximum allowed value of transverse momentum.

For $p_T^{max} >> 160$ MeV/c, we may write:

$$\overline{\Pi}(p_T) \simeq \frac{p_T}{0.0256} e^{-p_T/0.16}. \qquad (2)$$

Using this expression for $\overline{\Pi}(p_T)$, the average value of the transverse momentum of secondary particles produced in high-energy collisions may be calculated:

$$\langle p_T \rangle = 320 \text{ MeV/c}.$$

This in turn translates into an average production angle for secondary particles:

$$\langle \theta \rangle \simeq \frac{320}{p},$$

where θ is measured in mrad,

p is the momentum of the secondary particle measured in GeV/c.

Since this average production angle is inversely proportional to the momentum of the secondary particle, it is clear that accurate angle measurements will be increasingly important as beam momenta (and hence secondary particle momenta) are increased.

2. The total momentum of each secondary particle will depend upon the nature of the particle:

(a) Target nucleons will tend to be slow in the lab.

(b) At least one secondary particle will be fast in the lab--carrying off up to ~80% of the incident momentum.

(c) The remaining particles will be moderately energetic, possessing momenta $\lesssim$ 10 GeV/c.

Consequently, in order to be able to satisfactorily analyze collisions for beam momenta up to 50 GeV/c, one must be able to analyze secondary particles with lab momenta up to ~ 40 GeV/c.

Setting Errors

The final technical point to be considered before embarking upon a detailed discussion of each of the three chambers is to determine what setting error is to be assigned to each chamber. The ultimate resolution of any bubble chamber depends upon two types of factors:

1. Factors which are essentially random in nature and whose effect can therefore, in principle, be reduced through increasing the number of points measured on each track. Such factors include errors introduced by measuring-machine precision, errors introduced by finite bubble diameters, and random local variations in chamber constants which tend to average out over individual track lengths.

2. Factors which are systematic in nature but which are not sufficiently understood to be explicitly corrected for. Such factors include effects due to chamber turbulence, bubble drifts arising from the necessity of allowing time for adequate bubble growth, and errors introduced by insufficient knowledge of chamber optical constants and magnetic field. Errors of a systematic nature are clearly not reduced merely by increasing the number of points measured for a given length of track.

If we consider the net effect of both the above sources of error, then we can write for the effective chamber setting error:

$$\epsilon^2 = \epsilon_1^2/nL + \epsilon_2^2 \qquad (5)$$

where:

ϵ is the total chamber setting error

ϵ_1 is the setting error contribution due to random sources

ϵ_2 is the setting error contribution due to systematic sources

n is the number of measured points per unit length of track

L is the length of the track under consideration.

For the purposes of this report we make the assumption that n is made large enough so that ϵ_2 is the dominant contribution to ϵ. In Table II we present for each of the chambers being considered the minimum setting error which we believe to be attainable for that device.

For the 40-in. chamber we employed a rather optimistic value of ϵ in order to ascertain whether a small chamber had any chance of being useful at NAL. It is far from certain that such a small intrinsic setting error could be achieved for this chamber. (At present the 40-in. chamber operates with a setting error in the range of 60-70μ.)

The 80-in. chamber currently appears to possess a setting error in the range from 60-80μ. It is hoped that, with the expenditure of some effort and moderate expense, an ultimate value of 50μ could be obtained for this chamber. If this development fails to materialize, then the calculations carried out in this report for the 80-in. chamber should be modified accordingly.

The value of ϵ for the 12-ft chamber is based upon the appendix to report A.1-68-35 of the 1968 NAL Summer Study by L. R. Turner and agrees with that assumed by R. Kraemer and M. Derrick in the text of that report. In the absence of any test results from the 12-ft chamber, this estimate appears to be the most reliable number available to us. Should a different value of ϵ emerge once the 12-ft chamber is tested, then obviously some of our conclusions concerning this chamber may have to be modified.

Momentum and Angle Errors

The formulae for momentum and angle errors employed in this report are the following:[1]

$$\left(\frac{\delta p}{p}\right)^2 = \frac{1}{H^2}\left\{\frac{0.133\alpha}{L} + 3.55\left(\frac{p\epsilon}{L^2}\right)^2\right\} \tag{6}$$

$$\left(\frac{\delta\theta}{\langle\theta\rangle}\right)^2 = 10^{-8}\left\{1.47\,\alpha L + 141\left(\frac{p\epsilon}{L}\right)\right\}^2, \tag{7}$$

where

$\alpha = 1/\beta^2 \{\ell n\ 4.8\ p + \ell n\ 145\ \eta\}$

$= 20.0$ for 10 GeV/c pions

$= 22.8$ for 40 GeV/c pions

p is the particle momentum in GeV/c

θ is the particle production angle in radians

L is the track length in cm

ϵ is the chamber setting error in space, in μ

H is the chamber magnetic field in kG.

The above angle error formula assumes that the trajectory of the secondary track is perpendicular to the camera axes. For dipping tracks, $\delta\theta$ will in general be larger and related to the stereo angle between the chamber's cameras. This correction factor is less than two for most chambers even for tracks that are nearly parallel to one of the camera axes. For simplicity, therefore, we have here ignored this effect. It should be kept in mind, however, that Eq. (7) assumes an optimum configuration for measuring angles.

III. COMPARISON OF THE THREE CHAMBERS

Turning now to the analysis of the three bubble chambers under consideration, we shall find it convenient to conceptually divide each chamber into three distinct regions: 1) a beam-defining region, 2) an interaction region, and 3) a measurement region for secondary tracks. Let us now consider each of those regions separately.

Beam-Defining Region

In high-energy bubble-chamber experiments, beam momenta are most accurately determined through a knowledge of the beam system. Fractional momentum errors of ~0.1% are attainable in this manner. At present, beam track angles are determined within the bubble chambers themselves. Since at high energies these angles must be known to fair accuracy (as will be shown), the continued use of this technique will require increasingly larger beam-definition regions as beam momenta are increased--particularly for chambers with large setting errors.* A preferable procedure would be to determine these angles prior to the beam particle's entry into the chamber through the use of devices such as wire planes. It would then only be necessary to make a rough determination of beam track angles within the chamber itself (for purposed of correlating the external information with the internally measured events), and smaller beam-defining regions could be employed. For the purposes of this report, however, it was not assumed that such a system would be

*This class includes the planned 25-ft bubble chamber for which estimates of 500μ or more for the setting error have been made.

available (although we strongly urge that one be provided for all NAL bubble chambers), because we do not wish to digress into the very broad topic of hybrid systems.

Assuming, therefore, that beam track angles continue to be measured within bubble-chamber interiors, we can write for the transverse momentum error thus introduced:

$$\delta p_T = p\,\delta\theta \tag{8}$$

where:

- δp_T is the transverse momentum error introduced by lack of knowledge of the angles of the beam track
- p is the momentum of the beam track
- $\delta\theta$ is the uncertainty in the angle of the beam track. There will be an angle error in both the plane perpendicular to the camera axis and in the plane parallel to the camera axis. For the sake of simplicity, we here consider only the plane perpendicular to the camera axis; however, similar remarks apply to the parallel plane.

For 50 GeV/c incident particles, this uncertainty in transverse momentum can be written as:

$$\delta p_T = 5\left\{14.4\,(\epsilon/L)^2 + 0.0014L\right\}^{1/2} \tag{9}$$

where:

- δp_T is measured in MeV/c
- ϵ is measured in μ
- L is measured in cm.

Since we wish to make the beam-defining region as short as possible, the first term in the square root will dominate, yielding:

$$\delta p_T \simeq 19\,\epsilon/L.$$

Consequently, the length of the beam-defining region required to achieve a given uncertainty in transverse momentum will increase approximately linearly with setting error, and, as will be shown below, the magnitude of δp_T will greatly affect the chamber's ability to distinguish four-constraint events from other alternatives.*

Four-constraint events are identified by the degree to which they satisfy momentum and energy conservation. At high energies these constraints divide naturally into two groups: the two transverse momentum constants and the longitudinal

*A more detailed analysis of the question of 4c event identification is presented in Appendix A.

momentum and energy constraints. The utility of the latter two constraints will be limited by the size of the momentum error of the fast secondary tracks. These errors will in general be appreciable (as will be shown), and hence these constraints will not be of much use in discriminating against slow π^o mesons (up to several hundred MeV/c momentum). In contrast, to the extent that Eq. (1) is valid, the efficacy of the transverse momentum constraints will not diminish with increasing beam momentum. Using Eq. (1) for the transverse momentum distribution function for secondary π^o-mesons, we display in Table III the slow π^o contamination as a function of δp_T.

The total error in the transverse momentum balance for a given event will also contain contributions from the outgoing tracks, but since we shall be allowing a larger measurement region for these tracks (see below), the total value of δp_T will tend to be dominated by the contribution from the beam track.

If we set up a beam-defining region of 25 cm for the 80-in. chamber (which corresponds to a transverse momentum error contribution of ~ 40 MeV/c), then the corresponding region for the 40-in. chamber would be 20 cm, while for the 12-ft chamber, 125 cm would be required to achieve this same transverse momentum accuracy.

Interaction Region

Assuming an interaction mean free path in hydrogen of 277 m for σ = 1 mb, then the average number of beam tracks interacting in a given length of chamber is given by:

$$n = N(1 - e^{-\sigma L/277}) \qquad (11)$$

where:

- n is the number of beam particles interacting in the given region
- N is the total number of beam particles entering the region
- L is the length of the interaction region in m
- σ is the total cross section in mb for the beam particle.

The total number of beam tracks which can be tolerated in a single chamber expansion is clearly a function of the chamber's dimensions transverse to the beam. Since the 40-in. chamber is circular and has a 20-in. thin window, it can tolerate about as many beam tracks as the 80-in. chamber (~15/picture). The situation with the 12-ft chamber is less clear. However, since this chamber is longer than the 80-in., it will produce more interactions for the same number of beam particles admitted, thus increasing the chances for downstream confusion. Consequently, it is probably not unreasonable to also assume for the 12-ft chamber only 15 beam tracks per picture.

If we define a 75 cm long interaction region for both the 80-in. and the 12-ft chambers, this would imply that for 15 beam tracks and a total cross section of 25 mb, there would be on the average one acceptable interaction/picture for both chambers. This interaction rate is to be compared to a total interaction rate for these chambers of 2.5 interactions/picture for the 80-in. and 4.1 interactions/picture for the 12-ft, which is pertinent from the point of view of estimating the amount of confusion in the two chambers (high-energy collisions will in general yield a high multiplicity of charged secondary particles). In order to achieve a reasonable measuring accuracy in the 40-in. chamber, a shorter interaction length of only 30 cm (leaving 50 cm for the measurement of secondary tracks) is all that can reasonably be allowed. This implies only 0.4 interactions/picture which would mean that 60% of the pictures taken would be wasted. When this rate is compared to the total interaction rate for this chamber of 1.3 interactions/picture, it can be seen that rapid cycling and triggering the cameras would require a reasonably sophisticated setup to overcome this waste factor. Unless such a system is devised, however, it is difficult to see how the 40-in. chamber could be useful at NAL in light of this short interaction region.

Secondary Track Measurement Region

Having previously defined the beam and interaction regions we have approximately the following secondary track measurement regions available in each chamber: 0.5 m in the 40-in, 1.0 m in the 80-in., and 1.6 m in the 12-ft chamber. We summarize all of the previous region definitions in Table IV.

Having determined the length of the secondary track measurement region for each chamber, we are now in a position to compare the relative merit of each device for the type of reactions under consideration. If we differentiate Eq. (7) with respect to L, we can determine that an optimum length ($\mathcal{L}$) exists which minimizes the angle errors for any track:

$$\mathcal{L} = \left(\frac{191.3}{\alpha}\right)^{1/3} \left(\frac{p\epsilon}{1000}\right)^{2/3}$$

where:

$\mathcal{L}$ is given in cm.

In Table V we present for each chamber the optimum lengths for tracks of 10 and 40 GeV/c. These lengths are clearly larger than those available for the measurement of secondary tracks in all three chambers, thus indicating that it will be to our advantage to measure as much track length as is available for all but the slowest secondary tracks.

The transverse momentum of any secondary track is given by:

$$p_T = p \sin \theta \simeq p\theta. \tag{13}$$

Consequently, we can express any secondary track's contribution to the total error in an event's transverse momentum balance as:

$$\delta p_T = p_T \left\{ \left(\frac{\delta p}{p} \right)^2 + \left(\frac{\delta \theta}{\theta} \right)^2 \right\}^{1/2} . \tag{14}$$

For a track with average transverse momentum this becomes:

$$p_T = 320 \left\{ \left(\frac{\delta p}{p} \right)^2 + \left(\frac{\delta \theta}{\langle \theta \rangle} \right)^2 \right\}^{1/2} , \tag{15}$$

where here δp_T is measured in MeV/c. Table VI displays for each chamber the relative contribution of momentum and angle errors to the total transverse momentum error of a 40 GeV/c secondary track produced with the average value of transverse momentum. It can be seen from this table that:

1. The contribution to the total transverse momentum balance of any event from any secondary track is considerably less than the 40 MeV/c contributed by the beam track.

2. Angle errors tend to make the dominant contribution to δp_T, and hence little would be gained by increasing the magnetic field strengths. (The greatest benefit from such an increase would be obtained in the case of the 80-in. chamber since the contribution of the momentum and angle errors to δp_T are most nearly equal in this case.)

3. The 80-in. chamber has the minimum angle errors which lead also to the minimum transverse momentum errors for secondary tracks.

lII. MASS RESOLUTION

Based upon the information presented in Tables III and Vl, we hence conclude that it will be possible to separate out a sample of four-constraint events from events with missing π^o's right up to the highest beam momenta being considered in this report. We turn therefore to the question of what effective mass resolution can be obtained for these events. A separate analysis of the question of mass resolution based upon a slightly different set of assumptions is presented in Appendix B.

The effective mass of two secondary particles is given by:

$$M_{12}^2 = M_1^2 + M_2^2 + 2(E_1 E_2 - p_1 p_2 \cos \theta_{12}) \tag{16}$$

where

M_{12} is the effective mass of particles 1 and 2

M_j is the mass of particle j

E_j is the energy of particle j

p_j is the momentum of particle j

$\cos \theta_{12}$ is the cosine of the angle between particles 1 and 2.

For high-energy secondary particles [for which θ_{12} will be small by virtue of Eq. (4)], we can approximate Eq. (16) by:

$$M_{12}^2 \simeq M_1^2 + M_2^2 + p_1 p_2 \theta_{12}^2. \tag{17}$$

Consequently, the problem of measuring two-body effective masses at high energies is reduced to determining the quantity:

$$Q_{12}^2 = M_{12}^2 - M_1^2 - M_2^2 \simeq p_1 p_2 \theta_{12}^2. \tag{18}$$

The uncertainty in the determination of this parameter is given by:

$$\delta Q_{12} = Q_{12} \left\{ \frac{1}{4} \left[\left(\frac{\delta p_1}{p_1} \right)^2 + \left(\frac{\delta p_2}{p_2} \right)^2 \right] + \left(\frac{\delta \theta_{12}}{\theta_{12}} \right)^2 \right\}^{1/2}. \tag{19}$$

In order to estimate the magnitude of the term $\delta\theta_{12}/\theta_{12}$, let us consider the general dependence of $\cos \theta_{12}$ on the angles of particles 1 and 2:

$$\cos \theta_{12} = \cos \theta_1 \cos \theta_2 + \sin \theta_1 \sin \theta_2 \cos (\phi_1 - \phi_2) \tag{20}$$

where:

θ_{12} was defined in Eq. (16)

θ_j and ϕ_j are the polar and azimuthal angles of particle j about the beam direction.

For high-energy particles this can be approximated by:

$$\theta_{12}^2 \simeq \theta_1^2 + \theta_2^2 - 2\theta_1 \theta_2 \cos (\phi_1 - \phi_2). \tag{21}$$

If we wish to discuss a completely arbitrary two-body system (in contrast to discussing a particular state such as the ρ, for example), we can regard the angles θ_j and ϕ_j as each being independent which leads to the result:

$$\langle \theta_{12}^2 \rangle \simeq \langle \theta_1^2 \rangle + \langle \theta_2^2 \rangle \tag{22}$$

where we have averaged over ϕ_1 and ϕ_2. From Eq. (1) it can be shown that:

$$\langle \theta_j^2 \rangle = \frac{0.1536}{p_j^2} \tag{23}$$

where:

θ_j is the production angle in radians for particle j

p_j is the momentum of particle j in GeV/c.

Consequently, we find that it is the production angle of the slowest track which in general determines $\langle \theta_{12}^2 \rangle$. For purposes of estimation we may in fact write:

$$\left(\frac{\delta\theta_{12}}{\langle \theta_{12} \rangle} \right) \simeq \frac{\left\{ \frac{1}{p_1^2} \left(\frac{\delta\theta_1}{\langle \theta_1 \rangle} \right) + \frac{1}{p_2^2} \left(\frac{\delta\theta_2}{\langle \theta_2 \rangle} \right) \right\}}{\left(\frac{1}{p_1^2} + \frac{1}{p_2^2} \right)} . \tag{24}$$

In Table VII we present for each chamber the momentum and angle errors of a 10 GeV/c secondary track having average transverse momentum. Using Tables VI and VII we can discuss Eq. (19) in two limiting cases:

1. Two-body effective masses involving particles of approximately equal momenta in the range 10-40 GeV/c. Here angle error contributions to δQ_{12} tend to dominate--particularly in the cases of the 40-in. and 12-ft chambers.

2. Two-body effective masses involving particles of widely different momenta--e.g., one of 10 GeV/c and one of 40 GeV/c. In this case the momentum and angle contributions to δQ_{12} tend to be approximately equal. Two additional observations can be made:

1. Tracks which are slower than 10 GeV/c have momentum errors which are important relative to angle errors, but the absolute magnitude of these errors is not large and hence will not be the limiting factor in determining the utility of a bubble chamber at high energies.

2. The fractional error in Q_{12}, and hence roughly speaking in M_{12}, will be about 1-2% even without fitting, and hence will not be excessive for low-mass states (such as those most readily produced by diffractive processes). The effect of fitting will tend to decrease this error. In particular, fitting may be expected to affect most directly the momentum error of the fast tracks since, in the absence of any external method of measuring beam angles, the energy and longitudinal momentum of the beam will be in general better determined than the beam's transverse momentum. This will result in a further reduction in the importance of momentum errors relative to angle errors in the determination of two-body effective masses.

The discussion of multi-body effective masses is more complicated, but qualitative arguments can be given to support the contention that they will depend upon momentum and angle errors in roughly the same manner as has been discussed for the two-body case (see Appendix C).

From the foregoing analyses, we conclude that our ability to study single-vertex four-constraint interactions in bubble chambers at high energies will tend to be determined in large part by our ability to measure angles. This observation is clearly of importance to the determination of the desired value of chamber magnetic field for the analysis of reactions of the type being considered in this report. Since the chamber magnetic field is potentially an adjustable parameter, let us now briefly consider this question in more detail.

Choice of Magnetic Field

Momentum and angle determinations for most secondary tracks produced at high energies will be measuring-error limited. For example, the lengths for which measuring and coulomb scattering contributions to momentum and angle errors ($\mathcal{L}_p$ and $\mathcal{L}_\theta$, respectively) become equal are given by:

$$\mathcal{L}_p = \left(\frac{26.69}{\alpha}\right)^{1/3}\left(\frac{p\epsilon}{1000}\right)^{2/3} \tag{25}$$

$$\mathcal{L}_\theta = \left(\frac{95.92}{\alpha}\right)^{1/3}\left(\frac{p\epsilon}{1000}\right)^{2/3} \tag{26}$$

where:

$\mathcal{L}_p$ and $\mathcal{L}_\theta$ are given in cm.

In Table VIII we display for tracks of 10 GeV/c and 40 GeV/c, and for each chamber in question, the lengths $\mathcal{L}_p$ and $\mathcal{L}_\theta$. In the extreme measuring-error limited region, a simple relationship exists for the ratio between momentum and angle errors:

$$\frac{(\delta p/p)_m}{(\delta\theta/<\theta>)_m} = \frac{15.9}{HL} \tag{27}$$

where:

H is the chamber magnetic field in kG

L is the track length in m.

Assuming the secondary track measurement regions defined previously, we can construct Table IX which presents for each chamber the magnetic field values at

which momentum and angle errors for a single track are matched assuming measuring error limitation. Several factors tend to make it desirable to increase the chamber magnetic field strengths above the values listed in this table:

1. Coulomb scattering makes some contribution to momentum and angle errors--particularly for the slower tracks. If we consider just the coulomb scattering contributions to the total errors, then we get:

$$\frac{(\delta p/p)_c}{(\delta\theta/<\theta>)_c} = \frac{30.1}{HL} . \qquad (28)$$

Hence, a higher field is necessary to equalize momentum and angle errors when contributions from coulomb scattering are important.

2. Angle errors from slower tracks can combine with momentum errors from faster tracks to limit effective mass resolution. This makes it desirable to reduce momentum errors relative to angle errors.

3. Even when momentum and angle errors are approximately equal there is still some advantage to be gained ($\sim\sqrt{2}$) by decreasing momentum errors relative to angle errors.

When each of these points is considered, it emerges that magnetic field strengths which are approximately twice those listed in Table IX are about optimum for each chamber. For the 40-in. and 12-ft chambers, the proposed and existing magnetic field strengths of 70 and 18 kG, respectively, are completely adequate. For the 80-in. chamber, however, increasing the magnetic field strength to 30-35kG would be a desirable improvement.

IV. CONCLUSION

We conclude from the calculations presented in this report that it would be a desirable step for the BNL 80-in. chamber to be moved to NAL as an interim chamber for use as soon as experimental beams become available. We further propose that this chamber's magnetic field should be increased to 30-35 kG, and that an effort be made to decrease its intrinsic setting error to 50μ. Our calculations indicate that with these improvements, the 80-in. chamber is the most suitable existing United States chamber for use in the analysis of single vertex four-constraint interactions in the beam momentum range of up to 50 GeV/c, and that it would in addition be of great value in carrying out survey experiments involving any single vertex events. While we believe the 12-ft chamber would be suitable, we base our preference for the 80-in. chamber on the following facts:

1. The 40-in. chamber is too small to have an adequate interaction region when employed in a non-hybrid system.

2. Both the 40-in. and 12-ft chambers have inferior angular resolutions when compared with the 80-in. chamber, and this significantly lessens their ability to analyze high-energy collisions.

3. The optical system of the 80-in. chamber is familiar to nearly every bubble-chamber group in the United States and hence strong-interaction physics at NAL energies could be immediately carried out were this chamber to be made available. In contrast, the optical system of the 12-ft chamber represents a change from previous chambers and would consequently necessitate extensive modifications in user scanning and measuring equipment. This would inevitably result in lengthening the time necessary to complete initial NAL bubble-chamber experiments.

Finally, independent informal estimates of the cost of this proposal made by SLAC (based upon their experience in moving the Berkeley 72-in. chamber, and upon their magnetic field improvement proposal for the 40-in. chamber), and by BNL (based upon tentative plans for moving the 80-in. chamber within the BNL site during 1971) differ by less than 20%, with both laboratories concluding that the movement of the 80-in. chamber, plus its installation at NAL with an improved magnetic field, could be accomplished for less than 2 million dollars.[2] Such an expense is indeed moderate when weighed against the important physics program which this funding would initiate.

REFERENCES

[1]Design Study for a High Magnetic Field Hydrogen Bubble Chamber for Use on Nimrod, Rutherford High Energy Laboratory, January 1967, Appendix I, pp. 29-43. The given formulae hold for flat tracks only--i.e. for tan $\lambda \approx 0$. This is a good approximation for fast secondary tracks.

[2]J. Ballam, private communication.

Table I. Chambers Considered in this Report for Potential Movement to NAL.

1.	SLAC	40-in. chamber
2.	BNL	80-in. chamber
3.	ANL	12-ft chamber

Table II. Minimum Chamber Setting Errors Assumed.

Chamber	Setting Error (μ)
40-in.	40
80-in.	50
12-ft	250

Table III. Percentage of Low Energy π^o-Mesons Not Excluded by Transverse Momentum Balance.

Total Error on Transverse Momentum Balance (MeV/c)	π^o Contamination in 4c Sample (%)
10	0.2
20	0.7
30	1.6
40	2.6
50	4.0
75	8.1
100	13.0

Table IV. Chamber Region Definitions.

Chamber	Beam Definition Region (m)	Interaction Region (m)	Secondary Track Measurement Region (m)
40-in.	0.20	0.30	0.5
80-in.	0.25	0.75	1.0
12-ft	1.25	0.75	1.6

Table V. Optimum Track Lengths for Minimizing Angle Errors.

Chamber	Length for p = 10 GeV/c (m)	Length for p = 40 GeV/c (m)
40-in.	1.15	2.77
80-in.	1.34	3.22
12-ft	3.91	9.41

Table VI. Relative Contribution of Momentum and Angle Errors to the Total Transverse Momentum Error of a 40 GeV/c Track with Average Transverse Momentum.

Chamber	Magnetic Field (kG)	$\delta p/p$ (%)	$\delta\theta/\langle\theta\rangle$ (%)	δp_T (MeV/c)
40-in.	70	1.76	3.82	13.5
80-in.	20	2.07	2.46	10.3
12-ft	18	4.16	7.46	27.3

Table VII. Momentum and Angle Errors for a 10 GeV/c Secondary Track with Average Transverse Momentum.

Chamber	Magnetic Field (kG)	$\delta p/p$ (%)	$\delta\theta/\langle\theta\rangle$ (%)
40-in.	70	0.55	1.06
80-in.	20	0.99	0.89
12-ft	18	1.27	2.03

Table VIII. Lengths at which Measuring and Coulomb Scattering Contributions to Momentum and Angle Errors Become Equal for Tracks of 10 and 40 GeV/c.

	$\lambda_{(m)^p}$		$\lambda_{(m)^\theta}$	
Chamber	10 GeV/c	40 GeV/c	10 GeV/c	40 GeV/c
40-in.	0.60	1.44	0.92	2.21
80-in.	0.69	1.67	1.06	2.56
12-ft	2.03	4.89	3.11	7.49

Table IX. Magnetic Field Values at which Fractional Momentum and Angle Errors are Matched.

(Measuring Limited Region)

Chamber	Magnetic Field (kG)
40-in.	31.8
80-in.	15.9
12-ft	7.9

APPENDIX A. CONTAMINATION OF EVENTS WITH ONE π^o IN 4c EVENTS

The analysis is based on the probability that a π^o event will satisfy energy and momentum balance if the errors on the measured quantities are considered. Using plausible assumptions we can expect < 1.5% of π^o events to fit a 4c hypothesis. It is possible to have this low level of contamination in the 80-in. chamber up to at least 60 BeV/c incident momentum.

The major factor is eliminating π^o events in the transverse momentum balance. We assume that the transverse momentum of the π^o will be given by the CKP formula

$$p(p_T) = p_T e^{-p_T/0.16} \tag{1}$$

where p_T is the transverse momentum measured in BeV/c. The fraction of π^o events with π^o transverse momentum p_T or smaller is given by

$$F(p_T) = 1 - e^{-(p_T/0.16)} - p_T/0.16\, e^{-(p_T/0.16)}. \tag{2}$$

$F(p_T)$ vs p_T is plotted in Fig. 1.

An event with a π^o will satisfy transverse momentum conservation as a 4c if the π^o transverse momentum is less than the uncertainty in the transverse momentum of the measured tracks. From Fig. 1 we see that if the uncertainty in the measured transverse momentum is 40 MeV/c, 2.6% of the π^o events would have this or smaller transverse momentum.

The measurements on the beam track contributes an uncertainty in the transverse momentum

$$\Delta p_T = p_b \Delta\theta, \tag{3}$$

where p_b is the beam momentum and $\Delta\theta$ is the uncertainty in the measured direction of the beam.

Figure 2 shows Δp_T for p_b = 60 BeV/c as a function of ℓ, the length of the beam track measured for various ϵ, the setting error. Two curves are shown, the solid curve using the conventional form of the error formulas, the dashed curve using the form of the error equation claimed by Fisher to be appropriate to HPD type measurement. For Δp_T = 40 MeV/c, $\ell \approx$ 40 cm for both error formulas.

The transverse momentum error for an outgoing track is given by

$$\Delta p_T = \left[p^2 \Delta\theta^2 + p_T^2 (\Delta p/p)^2 \right]^{1/2} \tag{4}$$

where p_T is the transverse momentum of the track. In trying to estimate Δp_T, we make the following approximations:

1. Since both terms in Eq. (4) are proportional to p^2, we consider only Δp_T of the fast outgoing track.

2. The fast track is assumed to have ~80% of the incident momentum, i.e., 50 BeV/c for 60 BeV/c incident.

3. p_T is replaced by its average value given by Eq. (1), viz. 320 MeV/c.

With the lengths available in the 80-in. chamber, the uncertainties are limited by measurement error rather than by multiple scattering.

Using HPD error formulas

$$\Delta p_T = \frac{p\epsilon}{\ell^{3/2}} \left[3.8 \times 10^{-6} + \frac{1.48}{H^2 \ell^2} \right]^{1/2}.$$

The contributions to Δp_T from the angle error and the momentum error are equal for $H\ell = 1.98 \times 10^3$ kG-cm. For H = 20 kG, ℓ = 100 cm while for H = 40 kG, ℓ = 50 cm.

With conventional error formulas

$$\Delta p_T = \left[\frac{p\epsilon}{\ell} \; 1.44 \times 10^{-7} + \frac{3.64 \times 10^{-\omega}}{H^2 \ell^2} \right]^{1/2}.$$

Here the errors are matched for $H\ell = 1.6 \times 10^3$ kG-cm. For H = 20 kG, ℓ = 80 cm while for H = 40 kG, ℓ = 40 cm.

In the 80-in. chamber it seems as though reasonable requirements on the unfit mass resolution require that ℓ = 100 cm and H = 35 kG though the field is less important. For ℓ = 100 cm and H = 35 kG we find

Δp_T = 16 MeV/c conventional error formula

= 8 MeV/c HPD error formula

(p = 50 BeV, ϵ = 75μ).

The error on transverse momentum will be dominated by the contribution from the beam track and so the beam track could be profitably measured to a greater length if single π^o cross sections are very large.

Energy Balance

If the particles are well identified (i.e., by ionization) positive separation of 4c and 1c events will be possible if the uncertainty in energy is $\leq m_{\pi^o}$ = 135 MeV. The energy uncertainty is approximately the uncertainty in the momentum of the fast track.

$$\Delta E \approx \frac{1.2\times10^{-2} p^2 \epsilon}{H\ell^{52}} .$$

For p = 50 BeV, ϵ = 75μ, and ΔE = 135 MeV we find

H = 20.0 $\quad$ ℓ = 233

H = 40.0 $\quad$ ℓ = 177 cm.

The lengths required are too large except in the 25-ft chamber.

The π^o is not expected to be at rest in the lab, but the energy distribution in the lab is model-dependent. We discuss a simple model.

The π^o we consider are those produced with small p_T. For these

$$E_L \approx \gamma E^*_{\pi^o} (1 \pm \beta\beta^*),$$

where

E_L = π^o lab energy

β, γ refers to the motion of the center-of-mass ($\beta \approx 1$, $\gamma \approx 5$ at 50 BeV/c)

β^*, γ^* refer to the velocity of the π^o in the center-of-mass

$E^*_{\pi^o}$ is the energy of the π^o in the center-of-mass.

We assume the reaction produces two low mass "fireballs," one from the incident particle and one from the target. Since these fireballs usually have low masses, their velocities are approximately the same as the velocities of the original particle. Also, since they are of low mass the velocity of the π^o in the rest system of the fireball is small, hence, for these events the velocity β^* of the π^o in the center-of-mass system is $\approx \beta$, the velocity of the center-of-mass. Thus the π^o will be very slow in the lab if it is emitted from the backward fireball in the center-of-mass system, or very fast if it is emitted from the forward fireball. The fast π^o presents no problem because there will be a large longitudinal momentum unbalance. Figure 3 shows the situation when the π^o goes backwards in the center-of-mass. In this case it is clear that unless the total outgoing energy is determined to better than 135 MeV, an event which really has a π^o will fit the corresponding 4c hypothesis without a π^o. This problem is how well as must measure the momentum of the fastest outgoing track. This cannot be done well enough in the 80-in. chamber for the longitudinal momentum constraint to be useful for slow π^o's.

From the above considerations we conclude that longitudinal momentum and energy cannot be sufficiently well measured to eliminate some contamination of the 4c events with events with backward π^o's. However, if the transverse momentum uncertainties are small the contamination will be small typically ~1.3% for Δp = 40 MeV/c. These small transverse momentum uncertainties can be realized with fairly short tracks provided that ϵ is similar to that obtained now.

APPENDIX B. EXPECTED UNFIT MASS RESOLUTION

The error on the unfit mass of two particles depends on the laboratory configuration of the tracks. Since we expect to study diffraction type processes we anticipate that there will be a fast track in the final state. We shall assume that it will have 80% of the incident momentum or ~50 BeV/c for 60 BeV/c incident.

The effective mass of two relativistic particles is $m_{12}^2 \approx p_1 p_2 \theta_{12}^2$.

From the relationship for transverse momentum (the CKP formula) the mean square angle a track makes with the beam track is

$$\langle \theta^2 \rangle = \frac{1.54 \times 10^5}{p^2}, \tag{1}$$

where p is in MeV/c. For the mean square angle between two tracks

$$\langle \theta_{12}^2 \rangle = 1.54 \times 10^5 \left(\frac{1}{p_1^2} + \frac{1}{p_2^2} \right). \tag{2}$$

If $p_1 >> p_2$,

$$\langle \theta_{12}^2 \rangle = \frac{1.54 \times 10^5}{p^2}. \tag{3}$$

If we replace θ_{12}^2 in Eq. (1) by its average value we find

$$m_{12}^2 \approx 1.54 \times 10^5 \left(\frac{p_1}{p_2} \right)^2 (\mathrm{MeV/c^2}).$$

With this assumption viz. $\theta^2 = \langle \theta^2 \rangle$ we have calculated δm_{12}^2 [a] as a function of m_{12}, ϵ, ℓ, H for p_1 fixed at 50 BeV/c. [b] The results are shown in Figs. 4-6.

For the 25-ft chamber there is not a significant reduction in δ_m for $\ell > 3$ m when going from 18 to 35 kG. Fields higher than 18 kG would be useful in the 80-in. chambers. It also should be noted that the three chambers 80-in., 12-ft, and 25-ft give comparable errors in δm when tracks are measured to the maximum reasonable lengths. [c]

The Effect of Fitting on Mass Resolution

After fitting, the error in the longitudinal momentum of the fast track will be the uncertainty in the beam momentum, about 0.1%. The error on the momentum of the other track as well as the angle between the tracks are less likely to be reduced. This will reduce the error on effective mass to that given by the $\delta\theta$ term and the error on the slow track. With this assumption we have computed the error in dipion

masses.* The results are shown in the following table. The importance of the magnetic field on the error in dipion mass is diminished from the effect on the unfit errors.

m(BeV)	H(kG)	ϵ (μ)	L(cm)	δm(MeV)	Chamber
0.5	18	75	100	12	80-in.
0.5	35	75	100	10	80-in.
0.5	18	250	200	17	12-ft
0.5	35	250	200	16	12-ft
0.5	18	500	400	17	25-ft
0.5	35	500	400	17	25-ft
1.5	18	75	100	12	80-in.
1.5	35	75	100	10	80-in.
1.5	18	250	200	14	12-ft
1.5	35	250	200	13	12-ft
1.5	18	500	400	18	25-ft
1.5	35	500	400	17	25-ft
2.5	18	75	100	18	80-in.
2.5	35	75	100	15	80-in.
2.5	18	250	200	21	12-ft
2.5	35	250	200	20	12-ft
2.5	18	500	400	28	25-ft
2.5	35	500	400	27	25-ft

Notes:

[a]The error formulas are as follows:

$$m_{12}^2 = p_1 p_2 \theta_{12}^2$$

$$\frac{\delta m_{12}^2}{m_{12}^2} = \left(\frac{\delta p_1}{p}\right)^2 + \left(\frac{\delta p_2}{p_2}\right)^2 + 4\left(\frac{\delta\theta}{\theta}\right)^2$$

$$\left(\frac{\delta p}{p}\right)^2 = \frac{2.66}{H^2 \ell} + \frac{1.44 \times 10^{-4} p^2 \epsilon^2}{H^2 \ell^5} \quad \text{(HPD) (A. 1-68-35)} \qquad (1)$$

or

$$= \frac{3}{H^2 \ell} + 3.55 \times 10^{-6} \left(\frac{p\epsilon}{H\ell^2}\right)^2 \quad \text{(non-HPD) (from Fisher)}$$

$$\delta\theta^2 = \frac{0.04}{p^2} + \frac{3.8 \times 10^{-6} \epsilon^2}{\ell^2} \quad \text{(HPD) (from A. 1-68-35)} \qquad (2)$$

*Conventional, i.e., not HPD, errors have been assumed in this calculation.

$$\delta\theta^2 = \frac{10.24\times10^{-3}}{p^2} \times \left[4.39\,\ell + 14.06\times10^{-6}\left(\frac{p\epsilon}{\ell}\right)^2\right]$$

(from Fisher)

[b]The errors have been calculated using both HPD and conventional error formulas.

[c]These estimates should not be taken as literal truth but they should be good to better than 10 MeV.

APPENDIX C.

The effective mass of a system of N particles may be written as:

$$M^2_{1\,2\,3.\,.\,.N} = \sum_j^N M_j^2 + \sum_{j}^{N} \sum_{k<j}^{N} Q^2_{jk}$$

where

$$Q^2_{jk} \simeq p_j\, p_k\, \theta^2_{jk}$$

for a system of high-energy secondary particles. If we define in analogy with Q^2_{12}:

$$Q^2_{1\,2\,3.\,.\,.N} = M^2_{1\,2\,3.\,.\,.N} - \sum_j^N M_j^2$$

then we have:

$$Q^2_{1\,2\,3.\,.\,.N} \simeq \sum_{j}^{N} \sum_{k<j}^{N} Q^2_{jk}.$$

Consequently, an N-body effective mass will in general depend upon N(N-1)/2 two-body effective masses. Not all of these will be independent, but we can obtain a qualitative understanding of the resolution of an N-body system by ignoring these correlations and writing:

$$\left(\frac{\delta Q_{1\,2\,3.\,.\,.N}}{Q_{1\,2\,3.\,.\,.N}}\right) \simeq \sum_{j}^{N} \sum_{\substack{k \\ k<j}}^{N} \left[\left(\frac{Q_{jk}}{Q_{1\,2\,3.\,.\,.N}}\right)^2 \left(\frac{\delta Q_{jk}}{Q_{jk}}\right)\right]$$

$$= \frac{\sum_{j}^{N} \sum_{\substack{k \\ k<j}}^{N} \left\{Q^2_{jk} \left(\frac{\delta Q_{jk}}{Q_{jk}}\right)\right\}}{\sum_{j}^{N} \sum_{\substack{k \\ k<j}}^{N} \left\{Q^2_{jk}\right\}}$$

$$= \left\langle \left(\frac{\delta Q_{jk}}{Q_{jk}}\right) \right\rangle_{jk}$$

where the average is taken over j and k with the weighting factor Q^2_{jk}. Consequently, we are justified in concluding that our discussion of the two-body case applies at least qualitatively to N-body systems as well.

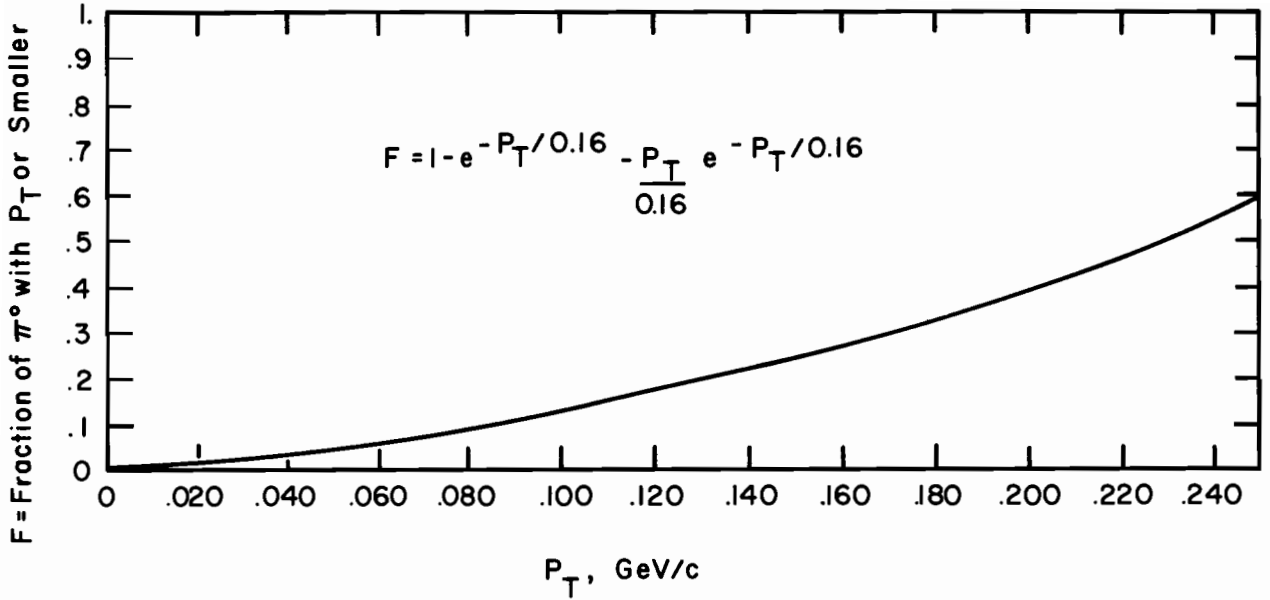

Fig. 1. Fraction of single π^o events having π^o's with transverse momentum p_T or smaller assuming the CKP formula.

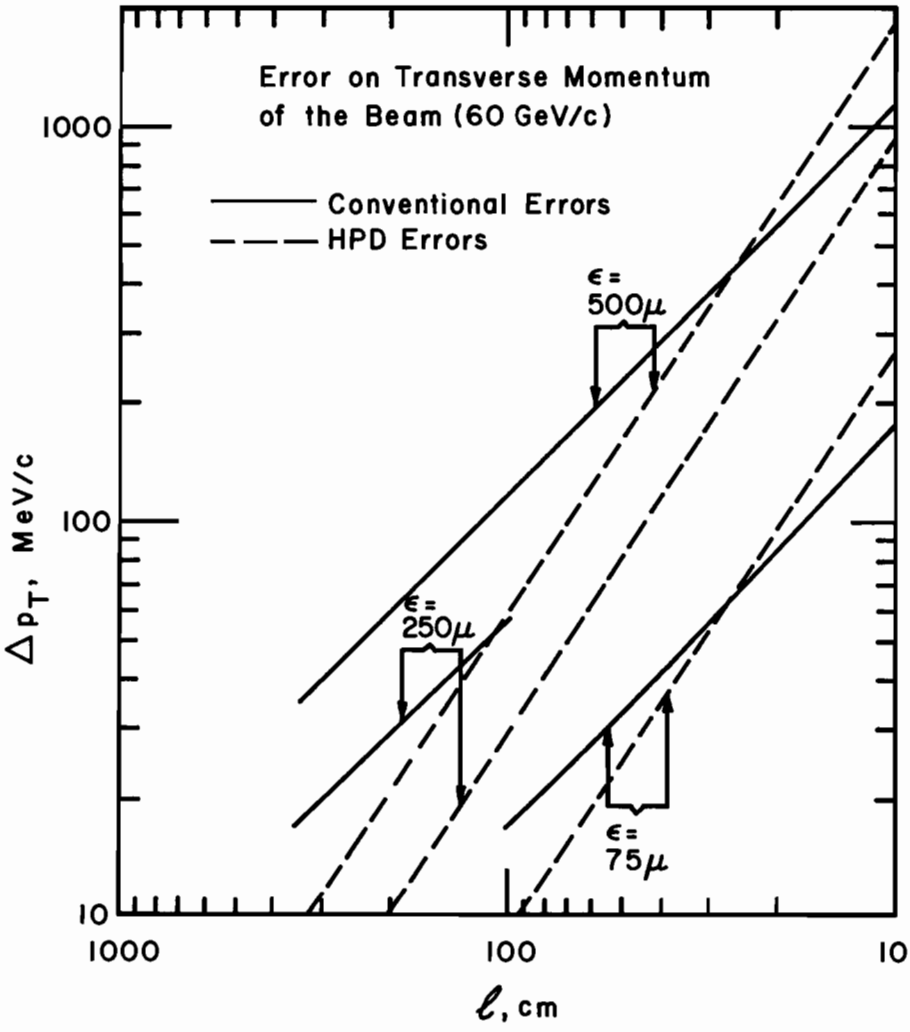

Fig. 2. Uncertainty in the transverse momentum of the beam as a function of measured beam length.

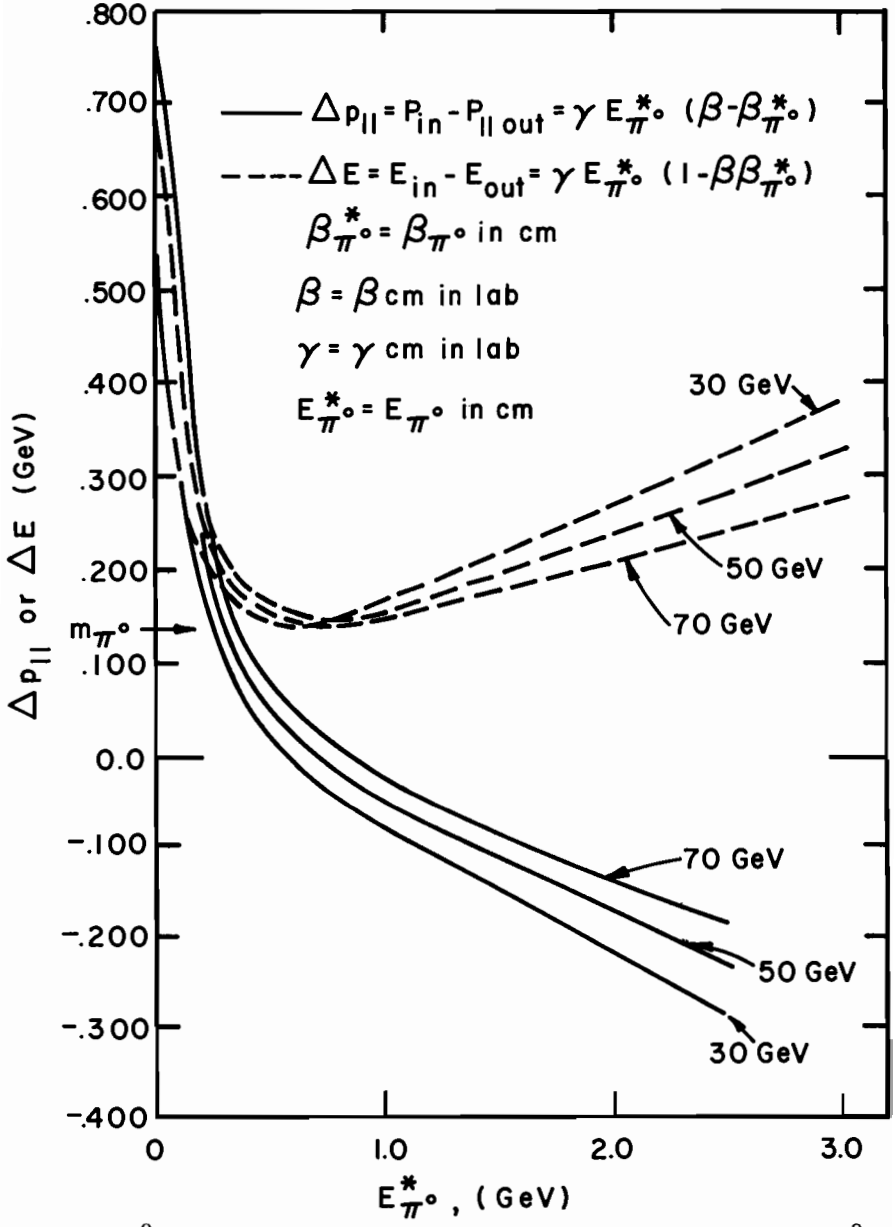

Fig. 3. π^o laboratory energy and longitudinal momentum errors as a function of π^o center-of-mass energy for various incident energies.

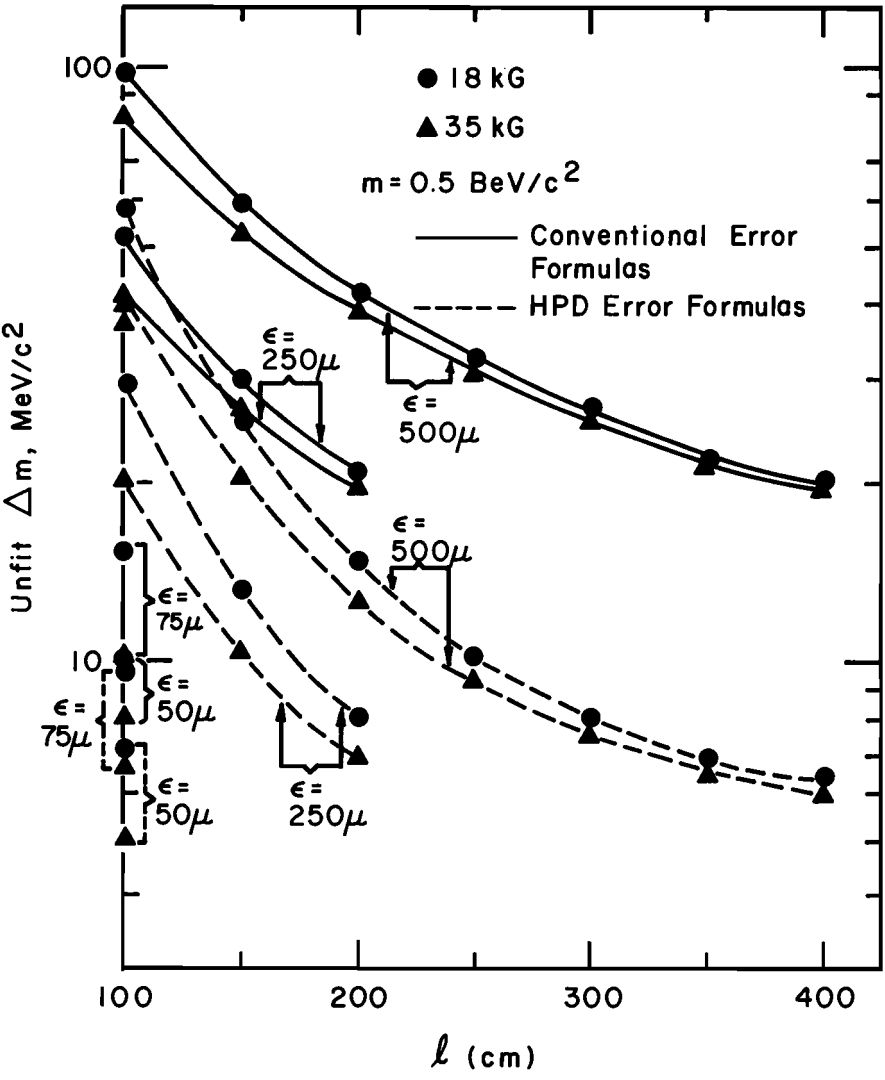

Fig. 4. Error on unfit dipion mass for a mass of 500 MeV/c^2 as a function of measured track length for different values of the setting error and magnetic field.

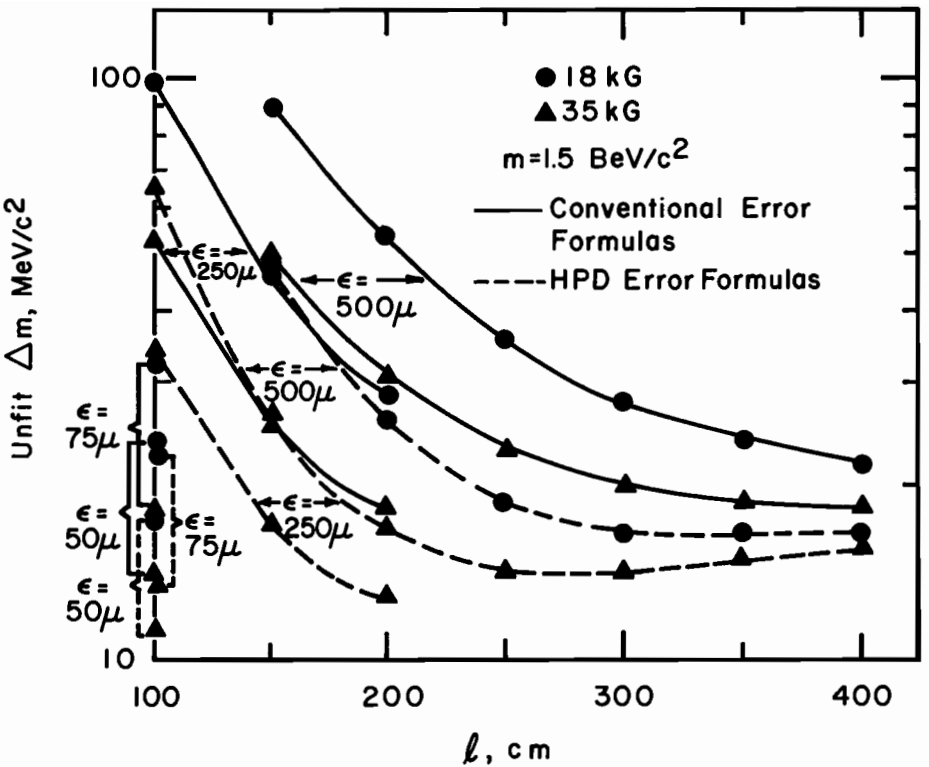

Fig. 5. Error on unfit dipion mass, for a mass of 1.5 BeV/c^2, as a function of measured track length, for different values of the setting error and magnetic field.

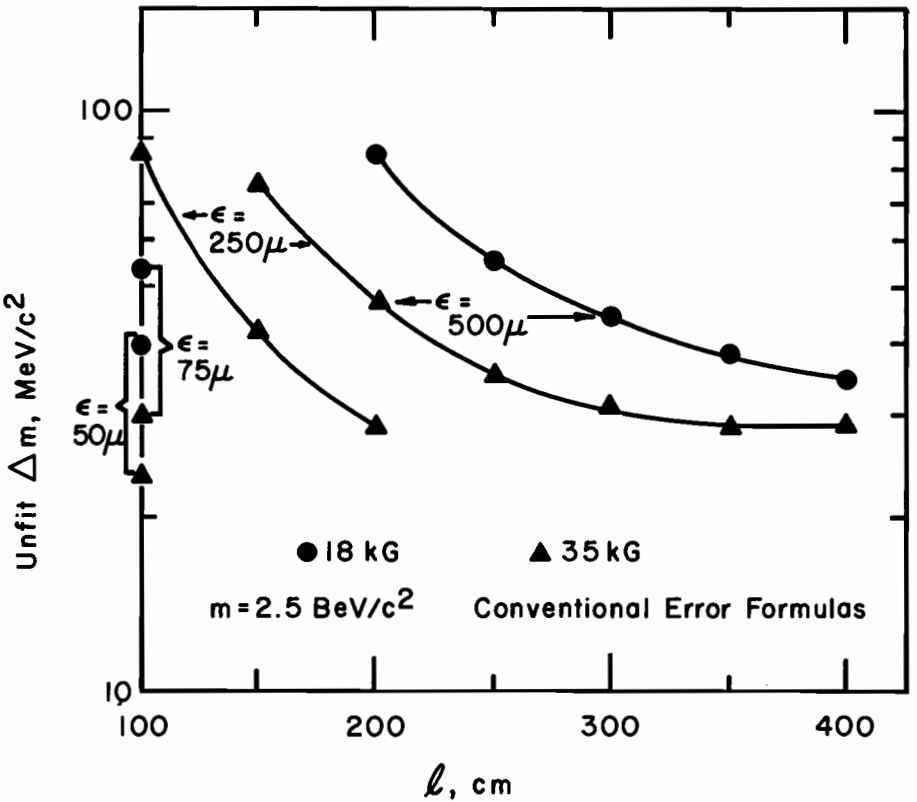

Fig. 6. Error on unfit dipion mass for a mass of 2.5 BeV/c^2, as a function of measured track length, for different values of the setting error and magnetic field.